Inorganic Chemistry Communications 188 (2026) 116456

Contents lists available at ScienceDirect

Inorganic Chemistry Communications

journal homepage: www.elsevier.com/locate/inoche

Research Article

Magnetically recyclable Fe_3O_4@SiO_2@GPTMS/2-aminophenol-Cu(II) nanocatalyst for green one-pot synthesis of 2-amino-4*H*-benzo[*b*]pyrans via solvent-free grinding technique

Sobhan Rezayati [a], Shaghayegh Fadaei [a], Maryam Manafi Moghadam [a], Ali Ramazani [a,b,*], Yavar Ahmadi [c,**], Guoying Zhang [d,**]

[a] The Organic Chemistry Research Laboratory (OCRL), Department of Chemistry, Faculty of Science, University of Zanjan, Zanjan 45371-38791, Iran
[b] The Convergent Sciences & Technologies Laboratory (CSTL), Research Institute of Modern Biological Techniques (RIMBT), University of Zanjan, Zanjan 45371-38791, Iran
[c] Department of Chemistry Education, Farhangian University, P.O. Box 14665-889, Tehran, Iran
[d] State Key Laboratory of Coal Conversion, Institute of Coal Chemistry Chinese Academy of Sciences, Taiyuan, Shanxi 030001, China

ARTICLE INFO

Keywords:
Fe_3O_4@SiO_2@GPTMS/2-aminophenol-Cu(II)
Hybrid organic-inorganic nanocatalyst
Mortar-pestle grinding technique
Knoevenagel–Michael cyclocondensation
2-Amino-4*H*-benzo[*b*]pyran derivatives

ABSTRACT

In response to the growing demand for sustainable catalysis in organic synthesis, this study introduces a novel, eco-friendly core-shell Fe_3O_4@SiO_2@GPTMS/2-aminophenol-Cu(II) magnetic nanocatalyst. The catalyst was synthesized via a straightforward procedure and thoroughly characterized using FT-IR, FE-SEM, TEM, EDX, TGA, VSM, XRD, and ICP techniques. TEM analysis confirmed a particle size distribution of 10–26 nm (average 31 nm), while TGA demonstrated excellent thermal stability, with 39.5% weight retention up to 800 °C. The nanocatalyst exhibited superior activity in the one-pot Knoevenagel–Michael Cyclocondensation of aromatic aldehydes, malononitrile, and dimedone under solvent-free, room-temperature mortar-pestle grinding conditions, yielding 2-amino-4*H*-benzo[*b*]pyran derivatives with excellent purity and yields (>90% in most cases). This method aligns with green chemistry principles through minimal waste, mild conditions, and low catalyst loading (1.3 mol%). Furthermore, its superparamagnetic properties facilitate easy magnetic recovery and reuse for at least five cycles with negligible loss in activity. This approach offers a versatile, efficient platform for heterocycle synthesis, emphasizing sustainability and recyclability.

1. Introduction

Industrial growth and the extensive production and use of various organic substances, while considered essential for the advancement of modern civilization, have led to a significant accumulation of persistent organic pollutants (POPs) in the environment. This has resulted in numerous environmental issues such as soil erosion, forest destruction, depletion of the ozone layer, climate change, and air and water contamination, all of which have serious impacts on human health and wildlife, leading to the decline of biodiversity [1–6]. Consequently, various regulatory agencies have urged the chemical industry to adopt synthetic strategies that align with the principles of green chemistry, rather than relying on conventional synthetic methods [7–9]. Recently, the application of green chemistry principles has emerged as a promising field. This approach aims to reduce energy consumption, use non-toxic materials and safer solvents, improve atom economy, and apply advanced catalytic methods [10].

Mechanochemical methods offer an efficient and eco-friendly alternative widely adopted in academia and industry. Mechanochemistry involves chemical reactions and structural transformations driven by mechanical energy [11]. This technique typically employs external mechanical forces to grind solid reactants, using devices such as shakers, ball mills, or mortar and pestle [12]. Grinding synthesis has garnered significant attention within green chemistry due to its solvent-free nature, particularly the avoidance of volatile organic solvents [13]. This approach not only reduces the generation of harmful byproducts but

* Corresponding author at: The Organic Chemistry Research Laboratory (OCRL), Department of Chemistry, Faculty of Science, University of Zanjan, Zanjan 45371-38791, Iran.
** Corresponding authors.
E-mail address: aliramazani@znu.ac.ir (A. Ramazani).

https://doi.org/10.1016/j.inoche.2026.116456
Received 12 September 2025; Received in revised form 26 February 2026; Accepted 3 March 2026
Available online 15 March 2026

also lowers overall costs [14,15], contributing to more sustainable chemical processes. When mechanochemical synthesis is combined with other methodologies, such as multicomponent reactions (MCRs), a synergistic effect arises. This integration leverages the advantages of both approaches, resulting in enhanced synthetic efficiency, minimized solvent waste and pollution, the ability to utilize insoluble starting materials, improved yields and product selectivity, and reduced reaction times [16].

Multicomponent reactions (MCRs) are synthetic processes that convert three or more readily available starting materials into a single product in a one-pot operation, making them among the most important reactions for the efficient formation of new C—C and carbon-heteroatom bonds in a single step [17]. MCRs, as a successful and rapidly expanding method for synthesizing complex molecules and increasing product diversity, are regarded as one of the most powerful approaches in the synthesis of natural products, organic materials, biologically active molecules, as well as pharmaceutical and agrochemical compounds. MCRs have gained significant attention due to their unique properties, including lower costs, simple operation, excellent selectivity, high atomic economy, high convergence, impressive yields, least waste production, and environmental friendliness [18–26]. One significant challenge in green chemistry is the development of catalysts with diverse features, such as high stability, eco-friendliness, recyclability, and reusability, particularly in synthetic organic processes like MCRs. In this context, the design, synthesis, and advancement of nanoparticles (NPs) have emerged as promising strategies [27,28].

Magnetic nanoparticles (MNPs) are becoming more important in many technological applications. Fe_3O_4-based MNPs have many benefits, including environmental safety, non-toxicity, superparamagnetic behavior, narrow size distribution, stability, high surface area, cost-effective production, dispersibility, and easy separation from reaction mixtures using an external magnetic field [29–31]. These nanoparticles also work well in several organic reactions [32–39]. Notably, silica improves reactivity, derivatization, and surface strength while being flexible. Silica-encapsulated Fe_3O_4 nanoparticles are popular due to their chemical inertness, low toxicity, mechanical and thermal stability, ease of functionalization, optical clarity, and easy production [40–43]. Researchers have focused on silica-coated Fe_3O_4 nanoparticles, especially for novel methods. Compared to bulk magnetic nanoparticles, their size and shape affect their performance, allowing them to perform better. The size and shape of magnetic nanoparticles greatly affect their properties. Adjusting reactant concentrations, capping agents, reaction time, and temperature to optimize nanoparticle dimensions is necessary to achieve desired characteristics. These nanoparticles' small nanoscale size improves surface-to-volume ratios and chemical potentials, making them crucial for catalysis.

Considerable efforts in both industry and academia have focused on creating innovative and efficient methods for synthesizing heterocyclic compounds [44–46]. Among these, benzopyrans (BZPs) and their derivatives stand out as a significant class synthesized via multicomponent reactions. The BZP framework is a vital natural scaffold present in plants, microorganisms, and animals, widely found in natural and edible sources, and exhibiting diverse pharmacological properties [47]. Although primarily produced synthetically for commercial use, BZPs are extensively applied across various industries including pharmacology, medical biochemistry, agriculture, and materials manufacturing. They are also used in perfumes, cosmetics, pigments, and as flavoring agents in food products like chocolate and baked goods [48–50]. Their greatest impact lies in medicinal chemistry, where they show promising pharmacological effects [51] such as anti-cancer, antimicrobial, anti-inflammatory, and potential treatment for neurodegenerative diseases like Parkinson's and Alzheimer's [52–56]. A notable compound, 2-amino-3-cyano-4H-pyran, is prized for its biological activities and can be efficiently synthesized via a one-pot, three-component reaction involving an aldehyde, 1,3-dicarbonyl compounds, and malononitrile in the presence of a catalyst [57,58]. Due to the importance of these

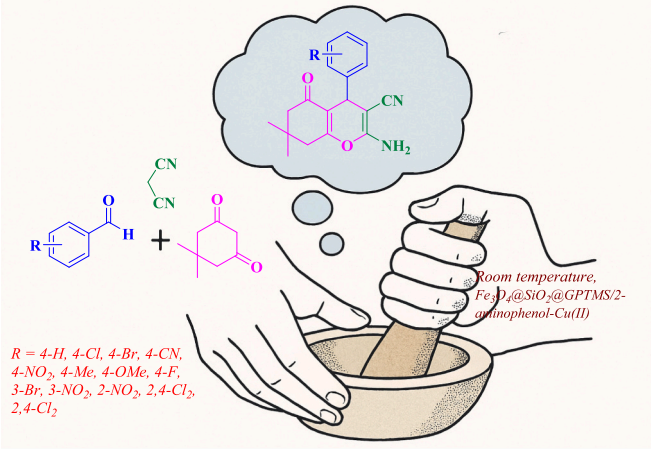

Scheme 1. Schematic representation of the synthesis of 2-amino-4*H*-benzo[*b*]pyrans derivatives

compounds, various catalysts such as Fe_3O_4@SiO_2@GPTMS@guanidine [59], GO-Fc@Fe_3O_4 [60], nano-SnO_2 [61], $[PEG(mim)_2][OH]_2$ [62], EDA/$(CH_2)_3$@SiO_2@Fe_3O_4 [63], and Fe_3O_4@NH_2@TCT@HOProCu [64] have been employed for this conversion. Despite the advantages of these methods, several suffer from drawbacks including extended reaction times, non-benign conditions, Substantial catalyst loading, High temperatures, utilization of volatile organic solvents, toxic catalysts, and non-recyclable catalysts.

Consequently, there is a need to develop a simple and recyclable catalyst for the synthesis of 2-amino-4*H*-benzo[*b*]pyran derivatives under mild and green reaction conditions. Herein, we have reported the development of Fe_3O_4@SiO_2@GPTMS/2-aminophenol-Cu(II) as an efficient heterogeneous magnetic nanocatalyst for the synthesis of 2-amino-4*H*-benzo[*b*]pyran derivatives via a solvent-free grinding reaction (Scheme 1).

2. Result and discussion

The catalyst was synthesized following the procedure outlined in Scheme 2 through a series of steps: First, Fe_3O_4 nanoparticles were generated using a coprecipitation method involving $FeCl_3$ and $FeSO_4{\cdot}7H_2O$. This was followed by the addition of TEOS to form the silica coating. Subsequently, GPTMS was employed as a linker and grafted onto Fe_3O_4@SiO_2, resulting in Fe_3O_4@SiO_2@GPTMS. This compound then facilitated the attachment of 2-aminophenol, producing Fe_3O_4@SiO_2@GPTMS/2-aminophenol. Finally, the resulting materials were treated with Cu species, leading to the formation of the superparamagnetic Fe_3O_4@SiO_2@GPTMS/2-aminophenol-Cu(II) via the coordination of NH_2 or OH ligands with Cu. The synthesized materials at each stage were analyzed using several methods, such as FT-IR, FE-SEM, TEM, EDX, TGA, VSM, XRD, and ICP.

FT-IR spectroscopic analyses were performed to determine the functional groups in the nanomaterials and to monitor and confirm the progressive alterations throughout the synthesis, surface modification of Fe_3O_4, and effective immobilization of SiO_2, GPTMS, 2-aminophenol, and Cu shells onto the Fe_3O_4 NPs (Fig. 1). The FT-IR analysis of the synthesized magnetite nanoparticles reveals a clear absorption peak at 580 cm^{-1}, which is linked to the Fe—O stretching vibration typical of the spinel structure associated with magnetite [65,66]. This absorption peak corresponds closely with earlier documented values for Fe_3O_4 nanoparticles, thus confirming the effective creation of nanoscale magnetite (Fig. 1a). Fig. 1b illustrates the FT-IR spectrum of silica-coated Fe_3O_4 nanoparticles, showing a broad absorption band at approximately 1166 cm^{-1}, indicative of the Si—O stretching vibration [65,66]. Subsequently, functionalization of Fe_3O_4@SiO_2 with GPTMS

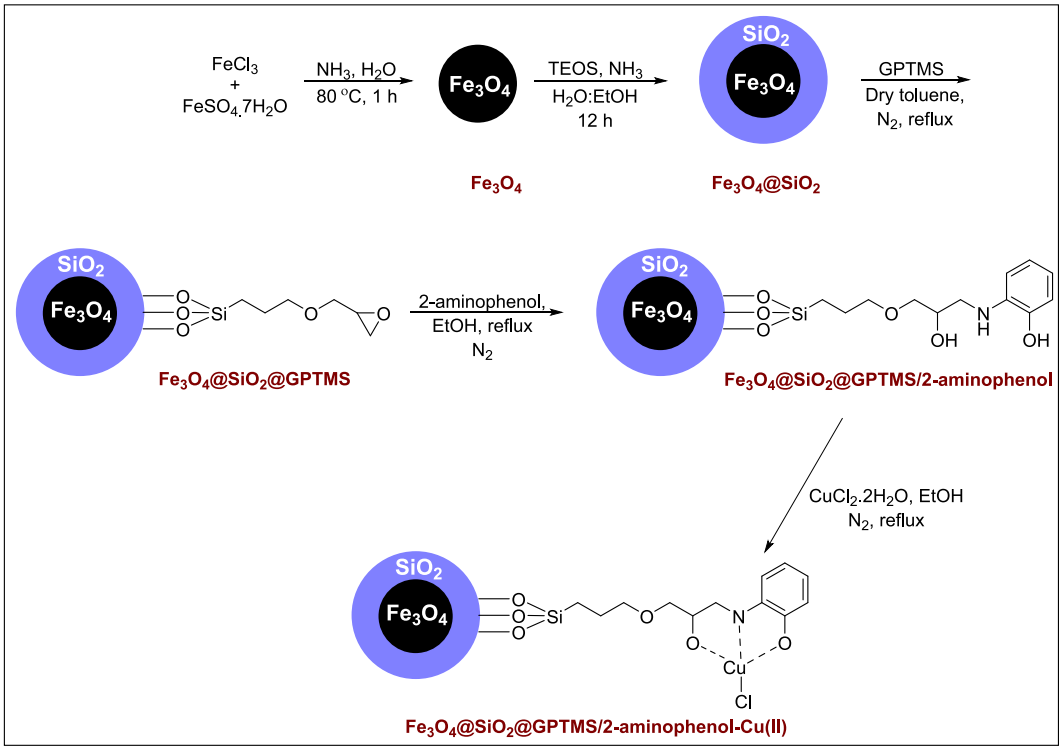

Scheme 2. Schematic representation of the synthetic route for Fe_3O_4@SiO_2@GPTMS/2-aminophenol-Cu(II)

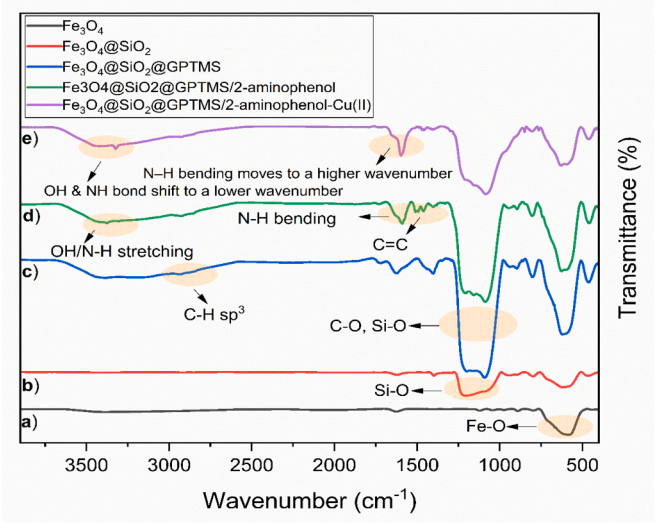

Fig. 1. FT-IR spectra of a) Fe_3O_4, b) Fe_3O_4@SiO_2, c) Fe_3O_4@SiO_2@GPTMS, d) Fe_3O_4@SiO_2@GPTMS/2-aminophenol, and e) Fe_3O_4@SiO_2@GPTMS/2-aminophenol-Cu(II) nanoparticles.

yielded GPTMS@SiO_2@Fe_3O_4, as shown in Fig. 1c. In the FT-IR spectrum, a new absorption band at 2933 cm^{-1} was observed, corresponding to the stretching vibration of the -CH_2 groups [65,67]. Additionally, an absorption band around 1210 cm^{-1}, attributable to the C—O bond of the epoxy group and overlapping with the strong silica absorption, was detected. The presence of these absorption bands confirms the successful incorporation of epoxy functionalities into the catalyst structure [65,67]. Upon finishing the fourth stage of the reaction, which involves the incorporation of 2-aminophenol, a peak indicative of the N—H stretching vibration of a primary amine emerges in the 3400–3500 cm^{-1} range. Furthermore, a peak at 1589 cm^{-1} is recognized as the N—H bending vibration. Peaks detected at 1460, 1509, and 1616 cm^{-1} are linked to the C═C stretching vibrations of the aromatic ring (Fig. 1d). Following the coordination of copper with 2-aminophenol, the stretching vibrations of the O—H bonds shift to a lower wavenumber (3322 cm^{-1}), while the N—H bending vibration moves to a higher wavenumber (1597 cm^{-1}) [65,66] (Fig. 1e). The changes and advancements noted in the IR spectrum from the initial magnetite to the end nanocatalyst distinctly illustrate the stepwise functionalization process, where each adjustment adds new vibrational bands yet preserves the fundamental structure of magnetite. The results and observations from this comprehensive spectroscopic investigation validate the successful creation of the Fe_3O_4@SiO_2@GPTMS/2-aminophenol-Cu(II) nanocatalytic system.

EDX analysis verified the presence of SiO_2, GPTMS, 2-aminophenol, and Cu shells on the Fe_3O_4 NPs, indicating the presence of N, C, O, Si, Fe, and Cu, with mass percentages of 0.95, 3.77, 25.47, 6.69, 60.63, and 2.49, respectively, as depicted in Fig. 2a. Moreover, elemental mapping analysis was utilized to acquire qualitative data on the distribution of components present in the synthesized catalyst (Fig. 2b). The resulting maps distinctly illustrate a homogeneous distribution of Cu species throughout the matrix. Additionally, the associated data confirms the steady presence of N, C, O, Si, and Fe in the nanocatalyst, indicating that the targeted catalyst is formed consistently. Overall, these findings indicate the successful immobilization of SiO_2, GPTMS, 2-aminophenol, and Cu shell nanoparticles, leading to the effective creation of the nanocatalytic system. In addition, the precise Cu concentration in the final nanocatalyst was assessed using the ICP method. The ICP results revealed that the true amount of Cu in the nanocatalyst was measured at 2.7 wt% (w%).

P-XRD analysis was conducted to explore the crystalline structure of the Fe_3O_4, Fe_3O_4@SiO_2, and Fe_3O_4@SiO_2@GPTMS/2-aminophenol-Cu (II) nanocatalyst (Fig. 3). The P-XRD pattern of the nanocatalyst reveals diffraction peaks at approximately $2\theta = 18.3°, 30.3°, 35.8°, 43.5°, 53.9°, 57.5°$, and $62.9°$, which are associated with the (111), (220), (311), (400), (422), (511), and (440) crystal planes. The sharp peaks reflect the highly crystalline structure of the nanoparticles. Because of the

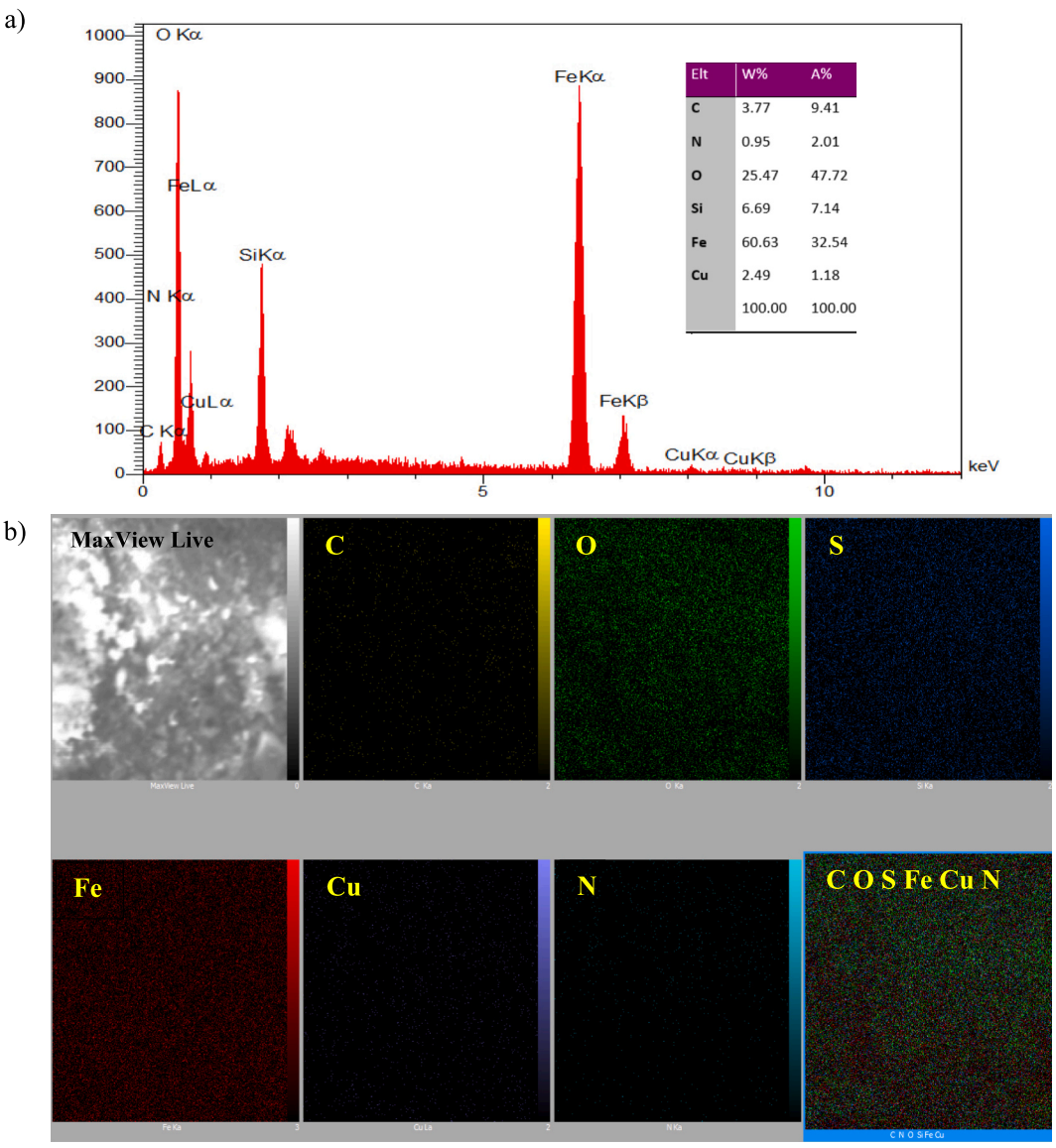

Fig. 2. a) EDX analysis and b) elemental distribution for the Fe_3O_4@SiO_2@GPTMS/2-aminophenol-Cu(II).

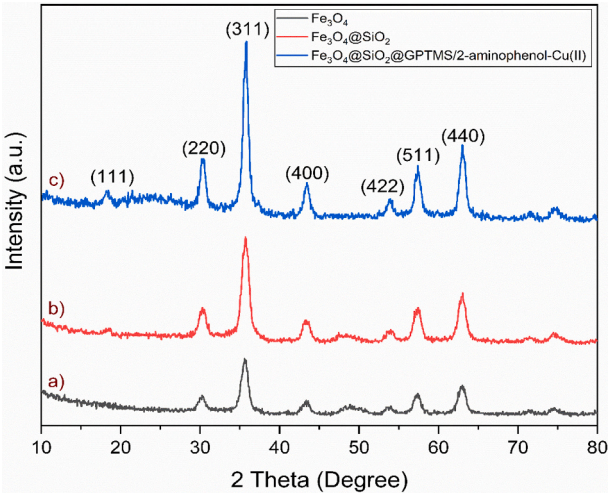

Fig. 3. P-XRD pattern for the a) Fe_3O_4, b) Fe_3O_4@SiO_2, and c) Fe_3O_4@-SiO_2@GPTMS/2-aminophenol-Cu(II).

Table 1
P-XRD data for the Fe_3O_4@SiO_2@GPTMS/2-aminophenol-Cu(II).

Number	Pos. [°2Th.]	FWHM Left [°2Th.]	d-spacing [Å]	Crystallite size (nm)
1	18.3	0.7872	4.83935	10.2
2	30.3	0.6888	2.94337	11.9
3	35.7	0.1968	2.50845	42.4
4	43.5	0.5904	2.07737	14.5
5	53.9	0.4920	1.69917	18.1
6	57.5	0.8856	1.60246	10.2
7	62.9	0.9840	1.47675	9.5
8	74.6	0.9840	1.27077	10.2

amorphous nature of SiO_2, the peak associated with SiO_2 was absent in the P-XRD pattern of the Fe_3O_4@SiO_2 and prepared (Fig. 3b and c). As per JCPDS 19–0629 [66], the synthesized nanoparticles exhibit a cubic morphology, with an average particle size of 15.87 nm, determined using the Scherrer equation. To further investigate the P-XRD data and Miller indices (*hkl*), the inter-planar distance of the final catalyst was examined. The Bragg equation [dhkl = k/(2sinθ)] allows for the calculation of this inter-planar distance, which was found to be 0.3225 nm.

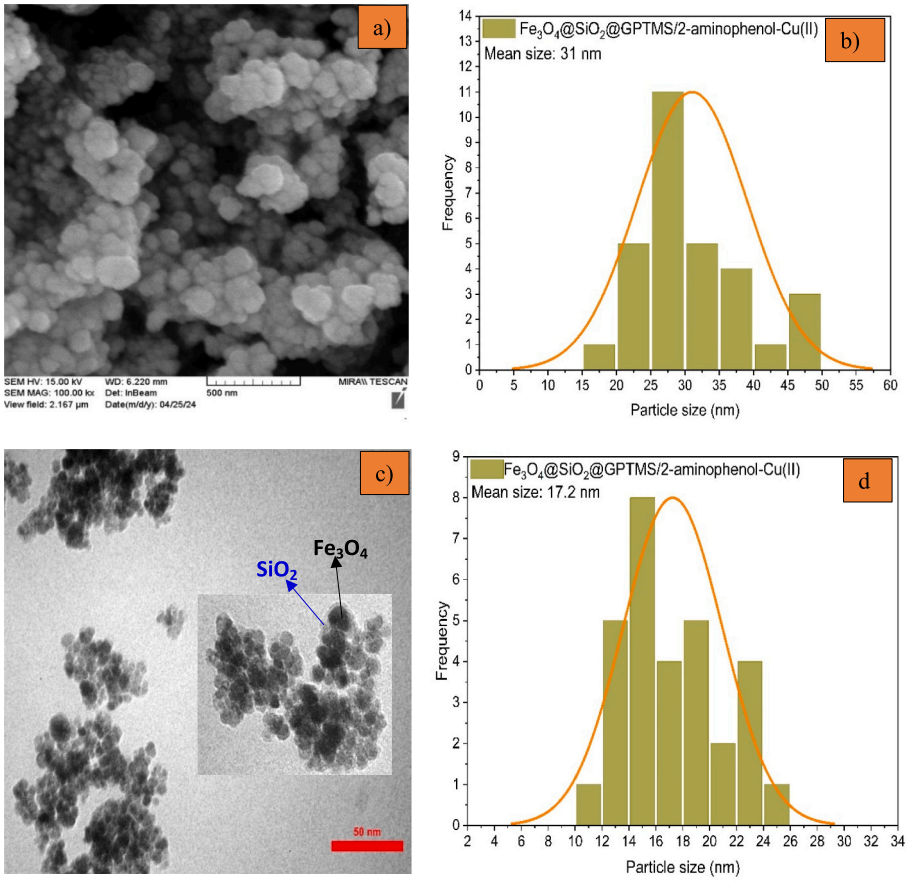

Fig. 4. a) SEM image and b) size distributions, c) TEM image and d) size distributions of the Fe_3O_4@SiO_2@GPTMS/2-aminophenol-Cu(II).

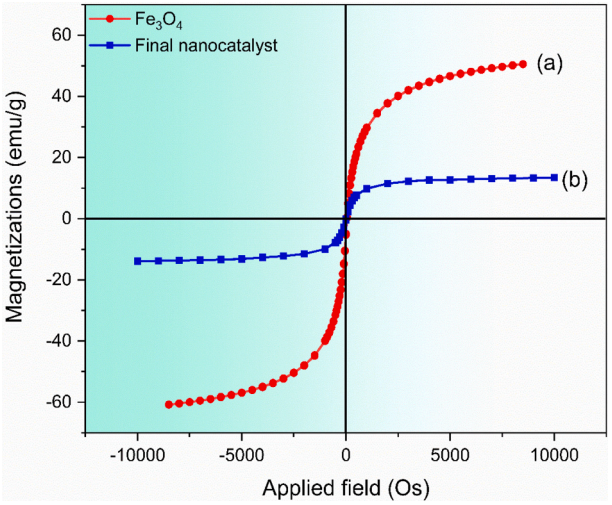

Fig. 5. VSM analysis for the a) Fe_3O_4 and b) Fe_3O_4@SiO_2@GPTMS/2-aminophenol-Cu(II).

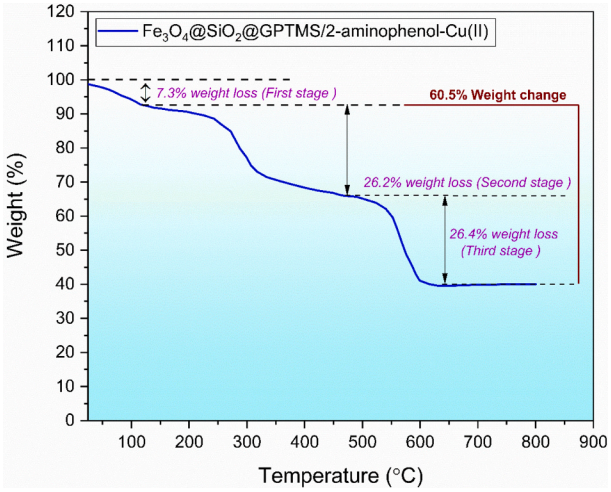

Fig. 6. TGA curve of the Fe_3O_4@SiO_2@GPTMS/2-aminophenol-Cu(II).

The corresponding Miller indices for this distance are detailed in Table 1.

The FE-SEM images and size distribution of the Fe_3O_4@SiO_2@GPTMS/2-aminophenol-Cu(II) nanoparticles, shown in Fig. 4a and b, reveal that the nanoparticles form spherical and uniform particles with an average size of about 35 nm, as indicated by the histogram. These results strongly suggest effective integration of the nanocatalyst onto the nanoparticles, which exhibit some irregular aggregation. Complementary TEM images and size distribution, presented in Fig. 4c and d, further confirm that the nanoparticles possess a clear core–shell structure with sizes ranging approximately from 10 to 26 nm. The darker core corresponds to Fe_3O_4, while the brighter shell represents the SiO_2 layer, demonstrating successful coating of Fe_3O_4 with silica. Together, these microscopic analyses validate the uniform morphology and core–shell architecture of the synthesized Fe_3O_4@SiO_2@GPTMS/2-aminophenol-Cu(II) nanocatalytic system.

In Fig. 5, the magnetic characteristics of Fe_3O_4 and Fe_3O_4@SiO_2@GPTMS/2-aminophenol-Cu(II) were analyzed with VSM. The VSM findings show that every sample demonstrates typical

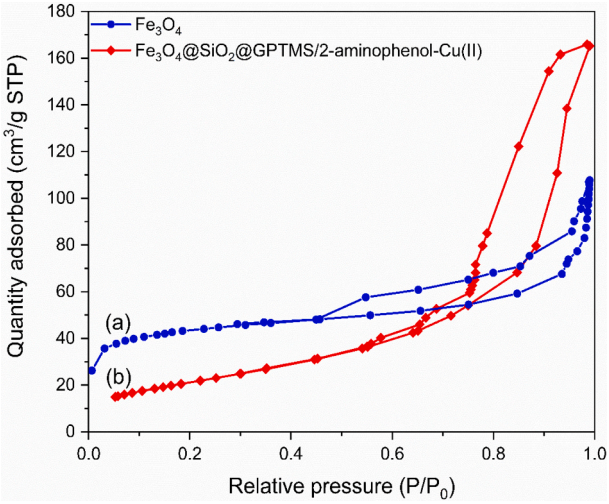

Fig. 7. Nitrogen adsorption–desorption of a) Fe_3O_4 and Fe_3O_4@SiO_2@GPTMS/2-aminophenol-Cu(II).

paramagnetic properties. The graph indicates a magnetization value of 50.5 emu/g for Fe_3O_4. For the prepared nanocatalyst, the magnetization is recorded at 13.4 emu/g, reflecting its magnetization. The decrease in the emu/g value confirms the deposition of nonmagnetic coatings, including SiO_2, GPTMS, 2-aminophenol, and Cu shells on Fe_3O_4 nanoparticles. Moreover, the synthesized nanocatalyst could be readily isolated from the reaction mixture with a strong external magnet, indicating that the sample exhibits superparamagnetic.

To assess the thermal stability and identify the organic and inorganic component content, TGA of Fe_3O_4 (Fig. S1, supporting information) and Fe_3O_4@SiO_2@GPTMS/2-aminophenol-Cu(II) (Fig. 6). TGA-DTA analysis of Fe_3O_4 conducted from 25 to 800 °C in air (at a rate of 10 °C/min) indicates a 16.95% weight decrease until approximately 400 °C: around 1–2% up to 100 °C due to the evaporation of surface moisture (attributed to its high surface area), and roughly 15% between 100 and 400 °C resulting from minor organic impurities or hydrates such as $Fe(OH)_2$. The weight stabilizes at 83%, suggesting a stable iron core (either pure Fe or its oxide) with no further oxidation. The DTA reveals endothermic peaks at approximately 39 °C and 60 °C related to the loss of volatiles, along with a broad endothermic peak for decomposition, with no exothermic reactions detected-this indicates high purity, thermal stability, and potential applicability in magnetic and catalytic fields. The Fe_3O_4@SiO_2@GPTMS/2-aminophenol-Cu(II) shows three steps to weight loss: (i) A preliminary slight weight reduction (approximately 7.73%) takes place under 110 °C as a result of the desorption of physically attached water molecules and surface humidity. (ii) Within the temperature interval of around 150–500 °C, a notable weight loss (i.e., 26.2%) is observed, likely resulting from the thermal breakdown of GPTMS and the 2-aminophenol coating, alongside the continued decomposition of leftover organic components. This finding suggests that the core−shell structure has been effectively stabilized with different organic compounds. (iii) The third stage of weight loss occurs at elevated temperatures ranging from 500 to 650 °C. Approximately 26.4% of the weight is lost during this stage. This reduction is attributed to the partial breakdown of molecules like silanol groups. Significantly, given that around 39.5% of the nanocatalyst's mass persists at 800 °C, we can deduce that roughly 60.5% weight loss transpires within this temperature range. This loss is primarily attributed to the decomposition and evaporation of the organic and volatile constituents in the nanocatalyst's framework, while the inorganic component remains predominantly stable.

Porosimetry assessments were performed on the Fe_3O_4 and Fe_3O_4@SiO_2@GPTMS/2-aminophenol-Cu(II) catalyst to evaluate their surface characteristics (Fig. 7). The N_2 adsorption-desorption isotherm for both Fe_3O_4 and Fe_3O_4@SiO_2@GPTMS/2-aminophenol-Cu(II) reveals a typical type-IV curve with a mesoporous configuration, demonstrating significant sorption hysteresis and pore compression. The surface area of Fe_3O_4 is significantly greater (162.5 m^2 g^{-1}) in comparison to Fe_3O_4@SiO_2@GPTMS/2-aminophenol-Cu(II) (79 m^2 g^{-1}). This indicates that the surface of Fe_3O_4 has been effectively coated with SiO_2, GPTMS, 2-aminophenol, and Cu layers. As shown by curve b, the pore structure of Fe_3O_4@SiO_2@GPTMS/2-aminophenol-Cu(II) appears cylindrical in shape. Nonetheless, the surface area of Fe_3O_4@SiO_2@GPTMS/2-aminophenol-Cu(II) is adequate for performing the intended functions.

Table 2
Optimization of the synthesis of **4b** using Fe_3O_4@SiO_2@GPTMS/2-aminophenol-Cu(II)[a].

Entry	Catalyst (g)	Conditions	Solvent	Time (min)	Yield (%)[b]
1	–	Grinding	–	60	trace
2	0.01	Grinding	–	15	81
3	0.02	Grinding	–	15	92
4	0.03	Grinding	–	10	94
5	0.04	Grinding	–	10	90
6	0.05	Grinding	–	10	90
7	0.03	–	H_2O	60	41
8	0.03	–	EtOH	180	90
9	0.03	–	EtOH: H_2O	160	87
10	0.03	–	CH_3OH	150	73
11	0.03	–	CH_3CN	180	39

[a] Reaction conditions: 4-chlorobenzaldehyde (1 mmol), dimedone (1 mmol), and malononitrile (1.2 mmol), various solvents (2 mL), and various amount of catalyst.
[b] Isolated yield.

Following an extensive characterization of the catalyst, its catalytic efficacy was investigated for the synthesis of 2-amino-4*H*-benzo[*b*]pyran derivatives using grinding conditions. Initially, the catalyst's performance was tested in a reaction comprising 4-chlorobenzaldehyde (1 mmol), dimedone (1 mmol), and malononitrile (1.2 mmol) to establish the best reaction conditions (Table 2). This involved a thorough evaluation of multiple factors, including reaction conditions, solvent choice and duration, as well as the amount of catalyst utilized. Without a catalyst under grinding conditions, the yield of **4b** was trace after 60 min (Table 2, entry 1). The reaction took place with 0.01 g of the catalyst under grinding conditions at ambient temperature. The findings indicated that the product yield steadily increased with longer reaction times, achieving a peak yield of 81% after 15 min (Table 2, entry 2). Given these findings, we chose to investigate the reaction using a larger quantity of catalyst under the same conditions to achieve improved yields (Table 2, entries 3–6). After conducting several tests, we noted that the optimal conditions for the reaction resulted in a yield of 94% when utilizing 0.03 g of the catalyst (Table 2, entry 4). Additionally, we raised the catalyst loading to 0.04 and 0.05 g, yet it did not influence the reaction efficiency (Table 2, entries 5 and 6). In the following research, we examined how various solvents influenced the reaction (Table 2, entries 7–11). Remarkably, utilizing ethanol as the solvent led to a substantial yield of around 90%, albeit over an extended duration of 180 min. In contrast, for all other solvents tested, there was no significant enhancement in either the reaction progress or yield during the same period. Furthermore, these results emphasize that the grinding conditions produced superior outcomes in contrast to solvent usage. This technique improved the reaction by augmenting the contact surface area and enhancing material dispersion, which in turn speeded up the reaction and greatly enhanced its efficiency.

In the subsequent section, we carried out a series of control experiments to assess the genuine active site and the true effectiveness of our developed catalyst system. For this purpose, we executed the reaction to synthesize 2-amino-4*H*-benzo[*b*]pyran derivatives using 4-chlorobenzaldehyde (1 mmol), dimedone (1 mmol), and malononitrile (1.2 mmol) under optimal conditions, employing materials produced at each

Table 3
Experiments designed to verify the true function of each catalyst component.

Entry	Catalyst	Conditions	Yield (%)
1	Fe_3O_4	Grinding/no solvent	50
2	Fe_3O_4@SiO_2	Grinding/no solvent	40
3	Fe_3O_4@SiO_2@GPTMS	Grinding/no solvent	9
4	Fe_3O_4@SiO_2@GPTMS/2-aminophenol	Grinding/no solvent	61
5	$CuCl_2.2H_2O$	Grinding/no solvent	42
6	Fe_3O_4@SiO_2@GPTMS/2-aminophenol-Cu(II)	Grinding/no solvent	94

stage of the catalyst development process (Table 3). As indicated in Table 3, the reactions involving Fe_3O_4 and Fe_3O_4@SiO_2 proceeded effectively, yielding only 53% and 40% of 4a, respectively (Table 3, entries 1 and 2). When Fe_3O_4@SiO_2@GPTMS was used, it resulted in a low yield of merely 11%, showing no significant enhancement (Table 3, entry 3). In contrast, the catalyst Fe_3O_4@SiO_2@GPTMS/2-aminophenol produced a yield of 61% of **4b** under same reaction conditions (Table 3, entry 4). A yield of 42% was obtained when the reaction utilized $CuCl_2{\cdot}2H_2O$ (Table 2, entry 5). These results highlight two crucial points: firstly, the copper species acts as the key active site within this catalytic system, primarily accounting for the elevated yield of the ester; secondly, the leaching of iron species from the core support into the solution is minimal and thus cannot operate as a Lewis acid catalyst.

Under optimal conditions, the synthesis of 2-amino-4*H*-benzo[*b*]pyran derivatives was investigated by reacting diverse aromatic aldehydes with dimedone and malononitrile. The results demonstrated that the reaction yielded excellent results for aromatic aldehydes featuring both electron-donating groups (like alkyl and alkoxy substituents) and electron-withdrawing groups (including nitro, halogen, and cyano), with product yields varying from 86% to 95%.

The capability of heterogeneous catalysts to be recovered and recycled using efficient and simple methods, along with their stability during repeated use, are essential aspects in the development and creation of these catalysts. Consequently, the subsequent stage of this research aimed at assessing the catalyst's stability and its recovery while reacting 4-chlorobenzaldehyde, dimedone, and malononitrile under optimized conditions (Fig. 8). Following each run, the catalyst was extracted from the reaction vessel with a magnetic bar and was subsequently rinsed with ethyl acetate to eliminate any products or leftover reactants. The catalyst was then used for the next run. Data showed that the catalyst exhibited outstanding dispersibility across multiple reactions after being separated from each run. Through this efficient and straightforward recycling method, our catalyst proved to be reusable in the reaction for as many as five cycles. While there was a minor decline in reaction yield, from 94% to 88%, this decrease was not substantial enough to compromise the catalyst's overall performance (Fig. 8a). In order to thoroughly assess the durability and structural integrity of the catalyst, a stringent series of analyses was performed following five consecutive reaction cycles. The retrieved catalyst was subjected to advanced characterization techniques such as FT-IR, SEM, and XRD (Fig. 8b-d). The SEM image illustrates that the catalyst preserves a consistent morphology and overall network integrity, indicating exceptional resilience against physical degradation (Fig. 8b). Supporting this, the FT-IR spectrum reveals minimal differences compared to the fresh catalyst, confirming that almost all functional groups and chemical stability are retained during reuse (Fig. 8c). Additionally, the XRD

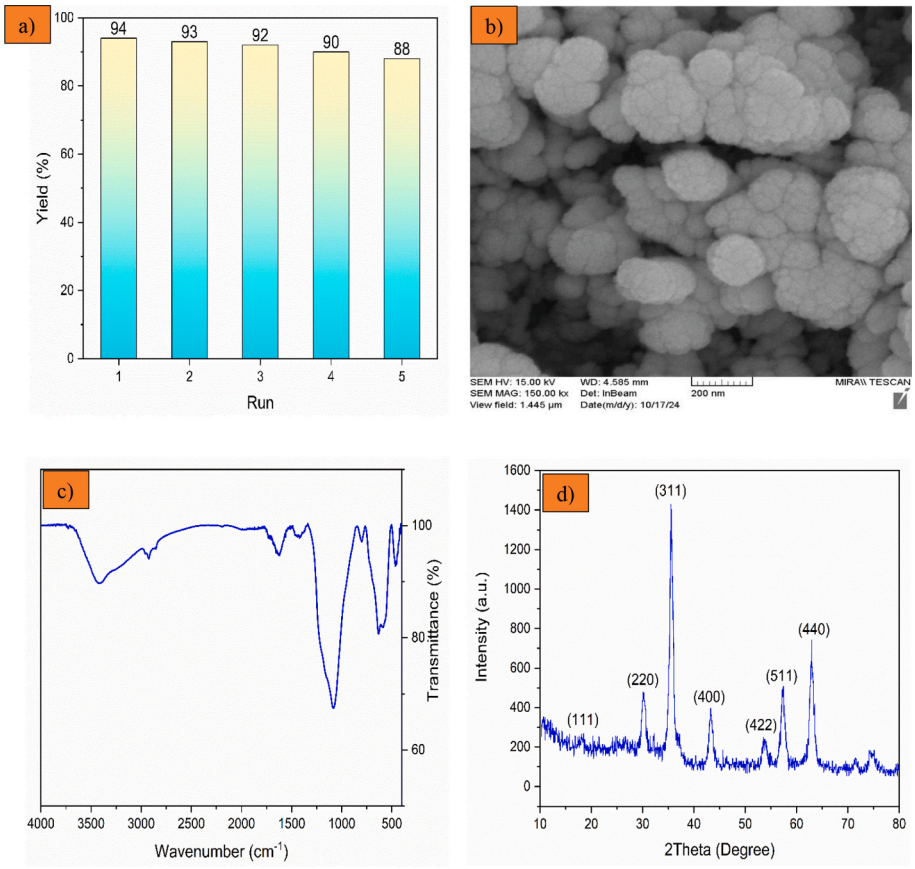

Fig. 8. a) Recovery of Fe_3O_4@SiO_2@GPTMS/2-aminophenol-Cu(II) catalyst for the synthesis of **4b**; b) SEM image, c) FT-IR spectrum, and d) PXRD pattern of the recovered material.

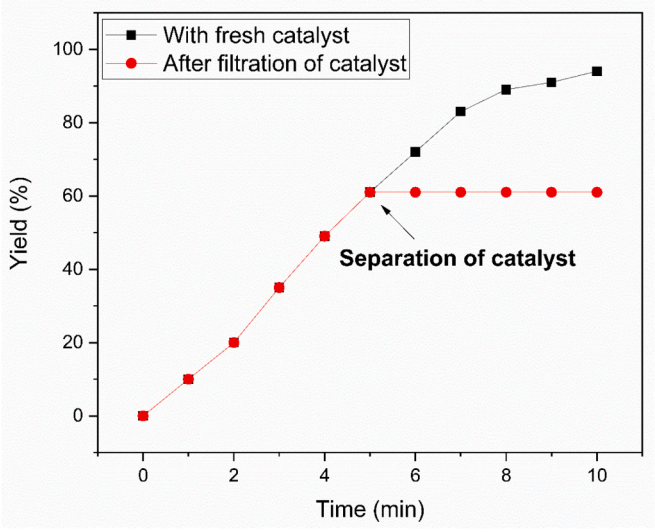

Fig. 9. Leaching test under optimized conditions for the synthesis of the **4b.**

pattern displays no substantial alterations, indicating that the crystalline structure of the catalyst remains unchanged throughout the recycling process (Fig. 8d). Collectively, these evaluations clearly underscore the catalyst's longevity and strong performance over several cycles.

The leaching test was conducted to evaluate the heterogeneous nature of the Fe_3O_4@SiO_2@GPTMS/2-aminophenol-Cu(II) catalyst utilized in the synthesis of 2-amino-4*H*-benzo[*b*]pyran derivatives (Fig. 9). Initially, the model reaction was carried out under optimized conditions. Midway through the reaction, the catalyst was removed from the reaction mixture using an external magnet, and the reaction was allowed to proceed in the absence of the catalyst for an additional half of the total reaction time. At the end of this period, no significant further conversion was observed. This strongly confirms the heterogeneity of the catalyst and indicates that no leaching of copper ions into the solution occurred. These findings underscore the stability and recyclability of the catalyst system in this synthetic process.

The proposed pathway for the synthesis of 2-amino-4*H*-benzo[*b*]pyran derivatives using the Fe_3O_4@SiO_2@GP/2-aminophenol-Cu(II) nanocatalyst is depicted in Scheme 3. First, the nanocatalyst interacts with the carbonyl group of aromatic aldehydes (1) and malononitrile (2). This interaction promotes the Knoevenagel condensation between the aldehyde and malononitrile, resulting in the loss of a water molecule and yielding the arylidene malononitrile intermediate (4). Moreover, the nanocatalyst enhances the reactivity of the methylene group in

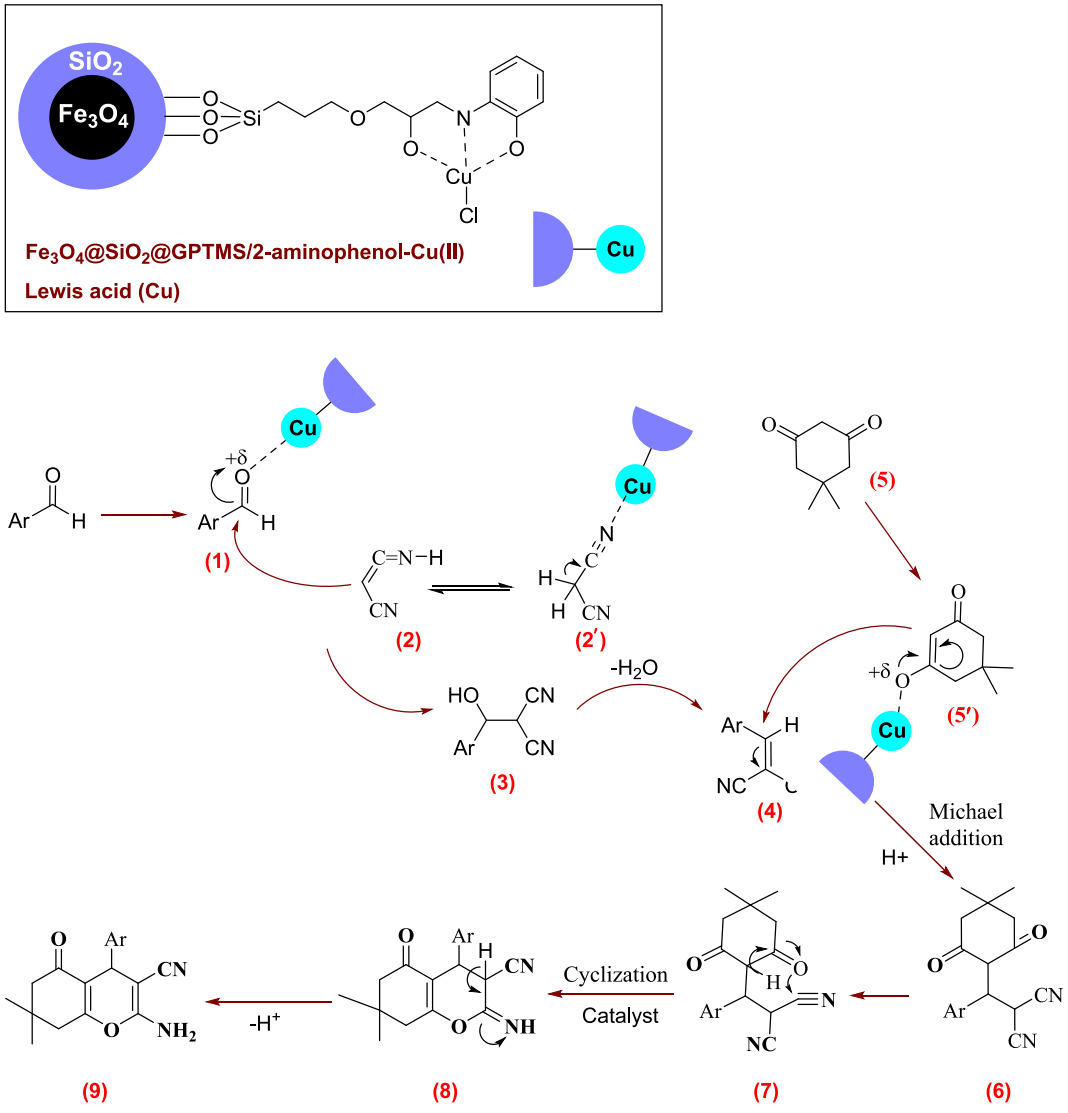

Scheme 3. Suggested catalytic route for producing 2-amino-4*H*-benzo[*b*]pyran

dimedone (5) for keto-enol tautomerization (5), which subsequently aids the Michael addition of intermediate (4) to dimedone, forming intermediate (6). Ultimately, cyclization reaction of intermediate **6** and hydrogen shift produced the 2-amino-4*H*-benzo[*b*]pyran derivatives **9**.

To demonstrate the effectiveness of the new catalyst, a comparative study was performed, evaluating it alongside other catalysts in the multicomponent synthesis of 2-amino-4*H*-chromenes. The detailed results are presented in Table 5. These results underscore the significant enhancements provided by our catalyst in optimizing reaction conditions. Specifically, using the Fe_3O_4@SiO_2@GPTMS/2-Aminophenol-Cu (II) catalyst resulted in shorter reaction times and lower temperatures while producing greater yields, showcasing its exceptional performance. Additionally, the reaction was conducted under grinding conditions, which improved its practicality and efficiency. In contrast, other previously reported methods required more stringent conditions, such as higher temperatures or extended reaction durations, highlighting the benefits of our methodology.

3. Experimental

3.1. Synthesis of Fe_3O_4@SiO_2

Fe_3O_4 nanoparticles were produced using a co-precipitation technique by mixing $FeSO_4{\cdot}7H_2O$ and $FeCl_3$ in water at 80 °C and gradually adding ammonia, resulting in black Fe_3O_4 formation. The mixture was stirred under a nitrogen atmosphere for 30 min and then allowed to sit at room temperature for 2.5 h. The magnetic Fe_3O_4 was then collected, cleaned, and dried. To create a SiO_2 coating, 1 g of Fe_3O_4 was dispersed in an ethanol-water solution through sonication, after which TEOS and an ammonia solution were introduced, and the mixture was stirred under nitrogen for 12 h. The resulting Fe_3O_4@SiO_2 core-shell particles were magnetically isolated, washed, and dried at 40 °C. A detailed description of the SiO_2@Fe_3O_4 synthesis can be found in the electronic Supporting Information (ESI) [65,66].

3.2. Synthesis Fe_3O_4@SiO_2@GPTMS

Li and colleagues introduced a simple approach to functionalize Fe_3O_4@SiO_2 nanoparticles with GPTMS, forming Fe_3O_4@SiO_2@GPTMS. In their method, 1 g of Fe_3O_4@SiO_2 was initially dispersed in 100 mL of dry toluene and sonicated for 20 min. Afterwards, 10 mmol of GPTMS was added gradually to the mixture, which was then refluxed under a nitrogen atmosphere at 80 °C for 8 h. Upon completion, the modified nanoparticles were separated magnetically, thoroughly washed twice with toluene (2 × 30 mL), and dried at room temperature overnight [67].

3.3. Synthesis Fe_3O_4@SiO_2@GPTMS/2-aminophenol

1 g of Fe_3O_4@SiO_2@GPTMS was initially dispersed in 30 mL of EtOH and sonicated for 20 min. Afterwards, 10 mmol of 2-aminophenol was added gradually to the mixture, which was then refluxed under a nitrogen atmosphere at 80 °C for 24 h. Upon completion, the modified nanoparticles were separated magnetically, thoroughly washed third with EtOH (3 × 20 mL), and dried at room temperature overnight.

3.4. Synthesis of the Fe_3O_4@SiO_2@GPTMS/2-aminophenol-Cu(II)

1 g of Fe_3O_4@SiO_2@GPTMS/2-aminophenol was dispersed in 30 mL of ethanol and placed in an ultrasonic bath for 20 min. Meanwhile, 0.43 g (2.5 mmol) of $CuCl_2{\cdot}2H_2O$ was separately dissolved in 20 mL of ethanol and quickly added to the catalyst mixture under vigorous stirring. The reaction was then carried out under nitrogen reflux for 24 h. After completion, the product was collected using an external magnet, washed several times with water and ethanol, and dried at room temperature to obtain Fe_3O_4@SiO_2@GPTMS/2-aminophenol-Cu(II).

Table 4
Reaction scope[a].

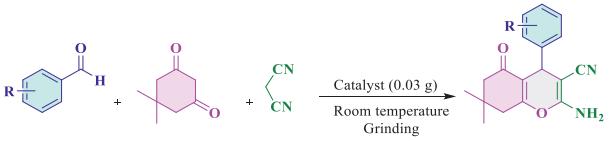

Entry	Products	Time (min)	Yield (%)[b]	M.p (°C) Found	M.p (°C) Reported
1	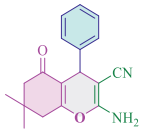 **4a**	18	87	231–234	233–235 [68]
2	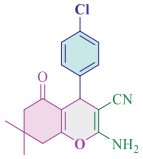 **4b**	10	94	213–216	214–216 [68]
3	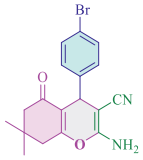 **4c**	10	91	217–220	221–223 [68]
4	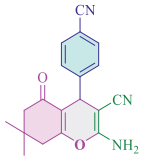 **4d**	10	95	228–230	224–227 [68]
5	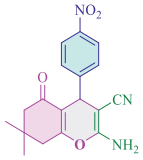 **4e**	10	92	180–182	179–181 [68]
6	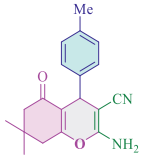 **4f**	20	86	219–221	218–220 [68]

(*continued on next page*)

Table 4 (*continued*)

Entry	Products	Time (min)	Yield (%)[b]	M.p (°C) Found	Reported
7	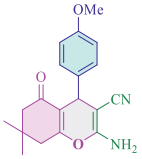 **4g**	20	90	199–202	200–202 [68]
8	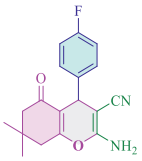 **4h**	10	88	185–188	187–188 [68]
9	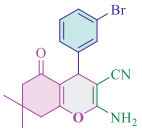 **4i**	15	92	215–218	225–228 [68]
10	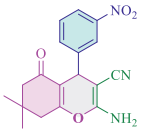 **4j**	12	93	213–216	212–213 [68]
11	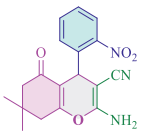 **4n**	10	93	220–222	222–223 [68]
12	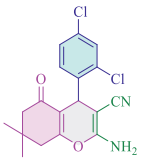 **4o**	15	93	179–180	177–178 [68]
13	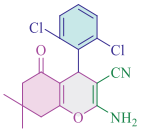 **4p**	15	92	249–251	249–251 [68]

[a] All reactions were conducted using different aldehydes (1 mmol), malononitrile (1.2 mmol), and dimedone (1 mmol) in the presence of Fe_3O_4@SiO_2@GPTMS/2-aminophenol-Cu(II) (0.03 g, 1.3 mol%) under grinding conditions at ambient temperature.

[b] Isolated yield.

Table 5
Evaluating the performance of the Fe_3O_4@SiO_2@GPTMS/2-Aminophenol-Cu(II) catalyst in synthesizing 2-amino-4*H*-chromenes derivatives compared to alternative catalysts.

Entry	Reaction conditions	Time (h)	Yield (%)	Ref.
1	LDH@PTRMS@NDBD@CuI (0.05 g), solvent-free, 40 °C	5–23 min	86–96	[69]
2	Mg/Al: 5.0 hydrotalcite (HT) (15 w%), H_2O, 80 °C	3–6	75–95	[70]
3	POPINO (5 mol%), H_2O, reflux	10–60 min	87–98	[71]
4	Sodium carbonate (5 mmol%), EtOH/H_2O, 25 °C	2	60–96	[72]
5	TPOP-2 (40 mg), solvent-free, 80 °C	4–6	82–88	[73]
6	Tungstic acid functionalized mesoporous SBA-15 (TAFMC-1) (30 mg), H_2O, reflux	11–15	77–86	[74]
7	Amino-appended β-cyclodextrin (a3) (0.05 mol), H_2O, r.t	5–24	82–95	[75]
8	$Fe(HSO_4)_3$ (0.1 mmol), refluxed in MeCN	3–5	82–94	[76]
9	PdRu@GO, H_2O:EtOH (2:1), 80 °C	12 min	88–95	[77]
10	solid base SiO_2-OK (0.09 mmol), solvent-free, 80 °C	1–8 min	79–95	[78]
11	Fe_3O_4@SiO_2@GPTMS/2-Aminophenol-Cu (II) (0.03 g), grinding, r.t	10–20 min	86–95	–

3.5. General mechanochemical synthesis of 2-amino-4H-benzo[b]pyrans derivatives

A variety of aromatic aldehydes (1 mmol), dimedone (1 mmol), malononitrile (1.2 mmol), and catalyst (0.03 g, 1.3 mol%) were combined in a mortar at room temperature for specified durations (see Table 4). Progress of the reaction was monitored by TLC. Once the reaction concluded, 5 mL of 95% ethanol was added to the mixture to dissolve the thick paste formed. The catalyst was conveniently removed using a magnet, then washed and dried for future use. Pure products were isolated from the reaction mixture by recrystallization in ethanol, and the melting points of the synthetic compounds were determined and compared to standard reference samples.

4. Conclusion

In this study, a novel eco-friendly magnetic nanocatalyst with a core-shell structure, Fe_3O_4@SiO_2@GPTMS/2-aminophenol-Cu(II), was successfully synthesized via a simple, green method. Comprehensive characterization using FT-IR, FE-SEM, TEM, EDX, TGA, VSM, XRD, and ICP confirmed its well-defined structure, uniform morphology, high thermal stability, and superparamagnetic properties. The nanocatalyst demonstrated exceptional activity in the one-pot Knoevenagel–Michael Cyclocondensation of diverse aromatic aldehydes, malononitrile, and dimedone under solvent-free grinding conditions at room temperature. This afforded the corresponding 4H-pyran derivatives in excellent yields (86–95%) and high purity within short reaction times (10–20 min), using minimal catalyst loading (0.03 g). Its superparamagnetic nature enabled facile magnetic separation and reuse for at least five cycles with minimal leaching and negligible activity loss (<6%), highlighting superior durability. The protocol aligns with green chemistry tenets by eliminating hazardous solvents, operating under mild conditions, and generating minimal waste. Overall, this hybrid organic-inorganic nanocatalyst emerges as a sustainable platform for synthesizing bioactive heterocycles, offering broad prospects in green organic synthesis applications.

Safety statement

No uncommon hazards are noted.

CRediT authorship contribution statement

Sobhan Rezayati: Writing – original draft, Project administration, Investigation. **Shaghayegh Fadaei:** Writing – original draft, Methodology, Data curation. **Maryam Manafi Moghadam:** Formal analysis, Data curation. **Ali Ramazani:** Writing – review & editing, Supervision, Project administration. **Yavar Ahmadi:** Writing – review & editing, Supervision. **Guoying Zhang:** Writing – review & editing, Software, Funding acquisition.

Declaration of competing interest

The authors declare that they have no known competing financial interests or personal relationships that could have appeared to influence the work reported in this paper.

Acknowledgements

This work is based upon research funded by Iran National Science Foundation (INSF) under project No.4033700 and the International Cooperation Bureau, Chinese Academy of Sciences (040GJHZ2024013MI).

Appendix A. Supplementary data

Supplementary data to this article can be found online at https://doi.org/10.1016/j.inoche.2026.116456.

Data availability

The data that has been used is confidential.

References

[1] R. Patnaik, Impact of industrialization on environment and sustainable solutions – reflections from a south Indian region, IOP Conf. Ser.: Earth Environ. Sci 120 (1) (2018) 012016.
[2] Y. Li, et al., Influence of industrialization and environmental protection on environmental pollution: a case study of Taihu Lake, China, Int. J. Environ. Res. Public Health 15 (12) (2018) 2628.
[3] Bakayoko, M., et al., Synthesis and characterization of the removal of organic pollutants in effluents. 2018. 33(2): p. 135–146, Rev. Environ. Health.
[4] O.M.L. Alharbi, et al., Health and environmental effects of persistent organic pollutants, J. Mol. Liq. 263 (2018) 442–453.
[5] O.A. Aluko, E.E. Osei Opoku, M. Ibrahim, Investigating the environmental effect of globalization: insights from selected industrialized countries, J. Environ. Manage. 281 (2021) 111892.
[6] Y.S. Kurniawan, et al., Green chemistry influences in organic synthesis : a review, Journal of Multidisciplinary Applied Natural Science 1 (1) (2021) 1–12.
[7] P.T. Anastas, T.C. Williamson, Green chemistry: An overview, in: Green Chemistry, American Chemical Society, 1996, pp. 1–17.
[8] K.N. Ganesh, et al., Green chemistry: a framework for a sustainable future, Environ. Sci. Technol. 55 (13) (2021) 8459–8463.
[9] R. Sheldon, D. Brady, Green chemistry, biocatalysis, and the chemical industry of the future, ChemSusChem 15 (2022).
[10] M. Bazargan, et al., Metal–organic framework-based sorbents in analytical sample preparation, Coord. Chem. Rev. 445 (2021) 214107.
[11] A.A.L. Michalchuk, et al., Tribochemistry, mechanical alloying, mechanochemistry: what is in a name? Front. Chem. 9 (2021) 685789.
[12] P. Baláž, E. Dutková, Fine milling in applied mechanochemistry, Miner. Eng. 22 (2009) 681–694.
[13] J.G. Hernández, C. Bolm, Altering product selectivity by mechanochemistry, J. Org. Chem. 82 (8) (2017) 4007–4019.
[14] O.V. Kharissova, et al., Greener synthesis of chemical compounds and materials, R. Soc. Open Sci. 6 (11) (2019) 191378.
[15] A. López-Lorente, et al., The ten principles of green sample preparation, TrAC Trends Anal. Chem. 148 (2022) 116530.
[16] M. Leonardi, M. Villacampa, J.C. Menéndez, Multicomponent mechanochemical synthesis, Chem. Sci. 9 (8) (2018) 2042–2064.
[17] I. Ugi, A. Dömling, W. Hörl, Multicomponent reactions in organic chemistry, Endeavour 18 (3) (1994) 115–122.
[18] A. Dömling, Recent developments in isocyanide based multicomponent reactions in applied chemistry, Chem. Rev. 106 (1) (2006) 17–89.
[19] A. Dömling, W. Wang, K. Wang, Chemistry and biology of multicomponent reactions, Chem. Rev. 112 (6) (2012) 3083–3135.
[20] Y. Gu, Multicomponent reactions in unconventional solvents: state of the art, Green Chem. 14 (8) (2012) 2091–2128.
[21] J. Sreelakshmy, K.B. Indulekha, E. Thomas, C.H. Suresh, Weak Interactions Break Strong Bonds: Noncovalent Complexes of H–X with N-Heterocycles, J. Phys. Chem. A 129 (22) (2025) 4835–4843.
[22] L.M. Kammer, M. Krumb, B. Spitzbarth, B. Lipp, J. Kühlborn, J. Busold, O. M. Mulina, A.O. Terentev, T. Opatz, Photoredox-catalyzed four-component reaction for the synthesis of complex secondary amines, Org. Lett. 22 (9) (2020) 3318–3322.
[23] B. Wang, S. Sun, J.T. Yu, Y. Jiang, J. Cheng, Palladium-catalyzed multicomponent reactions of O-alkynylanilines, aryl iodides, and CO2 toward 3, 3-diaryl 2, 4-quinolinediones, Org. Lett. 19 (16) (2017) 4319–4322.
[24] J. Li, Q. Zheng, A. Domling, Exploring phthalimide as the acid component in the Passerini reaction, Org. Lett. 26 (4) (2024) 829–833.
[25] Z.J. Kang, B.J. Han, Y.Q. Li, J.M. Shi, F. Teng, C.T. Feng, Copper-catalyzed Trifunctionalization of alkynes: one-pot assembly of antifungal Benzofuro [3, 2-d] pyrimidine-containing fused heterocycles, Org. Lett. 28 (2) (2025) 843–848.
[26] M.A. Tallarida, F. Olivito, C.D. Navo, V. Algieri, A. Jiritano, P. Costanzo, A. Poveda, M.J. Moure, J. Jiménez-Barbero, L. Maiuolo, G. Jiménez-Osés, Highly diastereoselective multicomponent synthesis of Spirocyclopropyl oxindoles enabled by rare-earth metal salts, Org. Lett. 25 (17) (2023) 3001–3006.
[27] A. Dandia, et al., Chapter 5 combination of green chemistry and magnetic nanocatalyst: A sustainable approach for the synthesis of value-added materials, in: S.V. Rajender, B. Bubun (Eds.), Volume 2 Industrial Applications, De Gruyter, Berlin, Boston, 2022, pp. 131–162.
[28] H. Veisi, et al., Recent advances in the application of magnetic nanocatalysts in multicomponent reactions, RSC Adv. 13 (30) (2023) 20530–20556.
[29] L. Babes, et al., Synthesis of Iron oxide nanoparticles used as MRI contrast agents: a parametric study, J. Colloid Interface Sci. 212 (2) (1999) 474–482.
[30] Singamaneni, S., et al., Magnetic nanoparticles: recent advances in synthesis, self-assembly and applications. J. Mater. Chem., 2011. 21(42): p. 16819–16845.
[31] S. Kango, et al., Surface modification of inorganic nanoparticles for development of organic–inorganic nanocomposites—a review, Prog. Polym. Sci. 38 (8) (2013) 1232–1261.
[32] Khojastehnezhad A, Gamraoui H, Jafari M, Peng Z, Moeinpour F, Siaj M. Size-dependent catalytic activity of palladium nanoparticles decorated on core–shell magnetic microporous organic networks. ACS Appl. Nano Mater. 2023 Sep 19;6 (19):17706–17.
[33] M. Keyhaniyan, A. Khojastehnezhad, H. Eshghi, A. Shiri, Magnetic covalently immobilized nickel complex: a new and efficient method for the Suzuki cross-coupling reaction, Appl. Organomet. Chem. 35 (4) (2021) e6158.
[34] R. Nemati, D. Elhamifar, A. Zarnegaryan, M. Shaker, Magnetic silica nanocomposite supported W6O19/amine: a powerful catalyst for the synthesis of biologically active spirooxindole-pyrans, Inorg. Chem. Commun. 145 (2022) 109934.
[35] P. Mofatehnia, D. Elhamifar, G.M. Ziarani, Cu-containing core–shell structured Fe3O4@ Gelatin nanocomposite: a novel catalyst for the preparation of hexahydroquinolines, Research on Chemical Intermediates. 49 (3) (2023) 967–978.
[36] N. Hosseininasab, A. Davoodnia, F. Rostami-Charati, A. Khojastehnezhad, Preparation, characterization, and first catalytic application of a novel phosphotungstic acid-containing ionic liquid immobilized on CuFe2O4@ SiO2 magnetic nanoparticles in the synthesis of 1 H-pyrazolo [1, 2-b] phthalazine-5, 10-diones, Russ. J. Gen. Chem. 87 (10) (2017) 2436–2443.
[37] S. Abaeezadeh, D. Elhamifar, Magnetic resorcinol-formaldehyde supported-DABCO as an effective and recyclable nanocatalyst, Sci. Rep. 15 (1) (2025) 22847.
[38] ZHAO, Y.; Zumin, Q.; Huang, J. Preparation and analysis of Fe3O4 magnetic nanoparticles used as targeted-drug carriers. Chin. J. Chem. Eng. 2008, 16 (3), 451–455.
[39] A.R. Sardarian, M. Zangiabadi, I.D. Inaloo, Fe3O4@SiO2/Schiff base/pd complex as an efficient heterogeneous and recyclable nanocatalyst for chemoselective N-arylation of O-alkyl primarycarbamates, RSC Adv. 6 (94) (2016) 92057–92064.
[40] T.T. Wen, L.Z. Wang, CoFe2O4@ SiO2@ APTES@ HO-PBA@ cu (OAc) 2: a highly efficient and recyclable nanocatalyst for one-pot synthesis of multifunctional 1, 5-benzodiazepines via three-component domino reaction, Materials Today Chemistry. 26 (2022) 101071.
[41] S. Paul, P. Barman, Rationally designed cu (ii) Schiff base metal complex anchored on NiFe 2 O 4@ chitosan: an efficient heterogeneous and magnetically retrievable hybrid nanocatalyst for the one-pot multi-component synthesis of bioactive 1-amidoalkyl-2-naphthols, Dalton Trans. 54 (5) (2025) 2132–2146.
[42] S. Sonei, F. Taghavi, A. Khojastehnezhad, M. Gholizadeh, Copper-functionalized silica-coated magnetic nanoparticles for an efficient Suzuki cross-coupling reaction, ChemistrySelect 6 (3) (2021) 359–368.
[43] Paul S, Sanjurani T, Gorai A, Barman P. NiFe 2O4@ SiO2-immobilized copper Schiff base complex as a versatile heterogeneous catalyst for efficient one-pot multicomponent synthesis of bioactive naphthopyran derivatives. React. Chem. Eng. 2025, 2025,10, 2121–2136.
[44] T. Eicher, S. Hauptmann, A. Speicher, The chemistry of heterocycles: structure, reactions, Syntheses, and Applications, 2003.

[45] A.T. Balaban, D.C. Oniciu, A.R. Katritzky, Aromaticity as a cornerstone of heterocyclic chemistry, Chem. Rev. 104 (5) (2004) 2777–2812.
[46] K. Nylund, P. Johansson, Heterocyclic compounds: Synthesis, properties and applications, 2010, pp. 1–389.
[47] F. Borges, et al., Simple coumarins and analogues in medicinal chemistry: occurrence, synthesis and biological activity, Curr. Med. Chem. 12 (8) (2005) 887–916.
[48] Boisde, P., WC Meuly in Kirk–Othmer Encyclopedia of Chemical Technology, Vol. 7. 1993, Wiley, New York.
[49] J.M. Dickinson, Microbial pyran-2-ones and dihydropyran-2-ones, Nat. Prod. Rep. 10 (1) (1993) 71–98.
[50] D. Cao, et al., Coumarin-based small-molecule fluorescent Chemosensors, Chem. Rev. 119 (18) (2019) 10403–10519.
[51] D. Srikrishna, C. Godugu, P.K. Dubey, A review on pharmacological properties of coumarins, Mini Rev. Med. Chem. 18 (2) (2018) 113–141.
[52] Konkoy, C., et al., Substituted 5-oxo-5, 6, 7, 8-tetrahydro-4H-1-benzopyrans and benzothiopyrans and the use there of as potentiators of AMPA. PCT Int. Appl. WO 0075123 2000. Chem. Abstr., 2001. 134: p. 29313a.
[53] I. Devi, P.J. Bhuyan, Sodium bromide catalysed one-pot synthesis of tetrahydrobenzo[b]pyrans via a three-component cyclocondensation under microwave irradiation and solvent free conditions, Tetrahedron Lett. 45 (47) (2004) 8625–8627.
[54] H. Gourdeau, et al., Antivascular and antitumor evaluation of 2-amino-4-(3-bromo-4,5-dimethoxy-phenyl)-3-cyano-4H-chromenes, a novel series of anticancer agents, Mol. Cancer Ther. 3 (11) (2004) 1375–1384.
[55] G. Zhang, et al., One-pot enantioselective synthesis of functionalized pyranocoumarins and 2-amino-4H-chromenes: discovery of a type of potent antibacterial agent, J. Org. Chem. 77 (2) (2012) 878–888.
[56] Y.B. Wagh, et al., A cesium fluoride promoted efficient and rapid multicomponent synthesis of functionalized 2-amino-3-cyano-4H-pyran and spirooxindole derivatives, Chin. Chem. Lett. 26 (10) (2015) 1273–1277.
[57] B. Maleki, S. Sheikh, One-pot synthesis of 2-Amino-2-chromene and 2-Amino-3-cyano-4H-pyran derivatives promoted by potassium fluoride, Org. Prep. Proced. Int. 47 (2015) 368–378.
[58] M. Partovi, et al., Recyclable mesalamine-functionalized magnetic nanoparticles (mesalamine/GPTMS@SiO2@Fe3O4) for tandem Knoevenagel–Michael cyclocondensation: grinding technique for the synthesis of biologically active 2-amino-4H-benzo[b]pyran derivatives, RSC Adv. 13 (48) (2023) 33566–33587.
[59] H. Taherkhani, et al., Grinding synthesis of 2-amino-4H-benzo[b]pyran derivatives catalyzed by highly efficient GPTMS/guanidine protected magnetic nanoparticles, ChemistrySelect 6 (41) (2021) 11362–11374.
[60] S. Mozaffarnia, R. Teimuri-Mofrad, M.-R. Rashidi, Synthesis of 2-amino-3-cyano-4H-pyran derivatives using GO-fc@Fe3O4 nanohybrid as a novel recyclable heterogeneous nanocatalyst and preparation of tacrine-naphthopyran hybrids as AChE inhibitors, J. Iran. Chem. Soc. 18 (2021).
[61] B. Baghernejad, M. Fiuzat, Synthesis of 2-amino-4H-pyran derivatives in aqueous media with nano-SnO2 as recyclable catalyst, Asian Journal of Nanoscience and Materials 4 (2) (2021) 171–177.
[62] M. Fallah-Mehrjardi, M. Foroughi, S.H. Banitaba, Polyethylene glycol-bis (N-methylimidazolium) dihydroxide as an efficient and recyclable basic phase-transfer catalyst for the synthesis of 4H-pyran derivatives in aqueous media, Asian Journal of Green Chemistry 4 (1) (2020) 75–86.
[63] S. Rezayati, et al., Mortar–Pestle Grinding Technique as an Efficient and Green Method Accelerates the Tandem Knoevenagel–Michael Cyclocondensation Reaction in the Presence of Ethylenediamine Immobilized on the Magnetite Nanoparticles, Polycycl. Aromat. Compd. 43 (7) (2023) 5869–5891.
[64] F. Kalantari, et al., Magnetic Nanoparticles Functionalized with Copper Hydroxyproline Complexes as an Efficient, Recoverable, and Recyclable Nanocatalyst: Synthesis and Its Catalytic Application in a Tandem Knoevenagel–Michael Cyclocondensation Reaction, Inorg. Chem. 60 (19) (2021) 15010–15023.
[65] Sobhan Rezayati, et al., Design of a Schiff base complex of copper coated on epoxy-modified core–shell MNPs as an environmentally friendly and novel catalyst for the one-pot synthesis of various chromene-annulated heterocycles, ACS Omega 6 (39) (2021) 25608–25622.
[66] Sobhan Rezayati, et al., Schiff base complex of copper immobilized on core–shell magnetic nanoparticles catalyzed one-pot syntheses of Polyhydroquinoline derivatives under mild conditions supported by a DFT study, Inorg. Chem. 63 (3) (2024) 1652–1673.
[67] Ahmet Ulu, et al., Design of epoxy-functionalized Fe3O4@ MCM-41 core–shell nanoparticles for enzyme immobilization, Int. J. Biol. Macromol. 115 (2018) 1122–1130.
[68] Kalantari, Fatemeh, et al. "Magnetic nanoparticles functionalized with copper hydroxyproline complexes as an efficient, recoverable, and recyclable nanocatalyst: synthesis and its catalytic application in a tandem Knoevenagel–Michael cyclocondensation reaction." Inorg. Chem. 60.19 (2021): 15010–15023.
[69] S. Paul, P. Barman, Rationally designed cu (ii) Schiff base metal complex anchored on NiFe 2 O 4@ chitosan: an efficient heterogeneous and magnetically retrievable hybrid nanocatalyst for the one-pot multi-component synthesis of bioactive 1-amidoalkyl-2-naphthols, Dalton Trans. 54 (5) (2025) 2132–2146.
[70] S.R. Kale, S.S. Kahandal, A.S. Burange, M.B. Gawande, R.V. Jayaram, A benign synthesis of 2-amino-4H-chromene in aqueous medium using hydrotalcite (HT) as a heterogeneous base catalyst, Cat. Sci. Technol. 3 (8) (2013) 2050–2056.
[71] M.G. Dekamin, M. Eslami, A. Maleki, Potassium phthalimide-N-oxyl: a novel, efficient, and simple organocatalyst for the one-pot three-component synthesis of various 2-amino-4H-chromene derivatives in water, Tetrahedron 69 (3) (2013) 1074–1085.
[72] Dinh Thanh N, Son Hai D, Thi Ngoc Bich V, Thi Thu Hien P, Thi Ky Duyen N, Thi Mai N, Thi Dung T, Thi Kim Van H, Ngoc Toan V, Huy NH, Thi Thanh Van T. Synthesis and structure of some substituted 2-amino-4-aryl-7-propargyloxy-4 H-chromene-3-carbonitriles. Synth. Commun. 2019 Jan 2;49(1):102–17.
[73] S.K. Kundu, A. Bhaumik, A triazine-based porous organic polymer: a novel heterogeneous basic organocatalyst for facile one-pot synthesis of 2-amino-4 H-chromenes, RSC Adv. 5 (41) (2015) 32730–32739.
[74] S.K. Kundu, J. Mondal, A. Bhaumik, Tungstic acid functionalized mesoporous SBA-15: a novel heterogeneous catalyst for facile one-pot synthesis of 2-amino-4 H-chromenes in aqueous medium, Dalton Trans. 42 (29) (2013) 10515–10524.
[75] Y. Ren, B. Yang, X. Liao, The amino side chains do matter: chemoselectivity in the one-pot three-component synthesis of 2-amino-4 H-chromenes by supramolecular catalysis with amino-appended β-cyclodextrins (ACDs) in water, Cat. Sci. Technol. 6 (12) (2016) 4283–4293.
[76] H. Eshghi, S. Damavandi, G.H. Zohuri, Efficient one-pot synthesis of 2-amino-4 H-chromenes catalyzed by ferric hydrogen sulfate and Zr-based catalysts of FI, Synth. React. Inorg., Met.-Org., Nano-Met. Chem. 41 (9) (2011) 1067–1073.
[77] B. Şen, N. Lolak, Ö. Paralı, M. Koca, A. Şavk, S. Akocak, F. Şen, Bimetallic PdRu/graphene oxide based catalysts for one-pot three-component synthesis of 2-amino-4H-chromene derivatives, Nano-Structures & Nano-Objects. 12 (2017) 33–40.
[78] E. Chandralekha, A. Thangamani, R. Valliappan, Efficient atom-economical solvent-free one-pot multicomponent synthesis of 2-amino-4 H-benzo [b] pyrans catalyzed by solid base SiO2-OK as a reusable catalyst, Res. Chem. Intermed. 41 (4) (2015) 1951–1966.

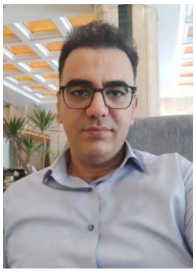

Sobhan Rezayati was born in 1988 in Ilam, Iran. He received his Bachelor's degree in Chemistry and Master's degree in Organic Chemistry in 2010 and 2012, respectively. He received his Ph. D. degree in 2022 from the University of the Zanjan under the supervision of Professor Ali Ramazani. His Ph.D. studies include the design and synthesis of various magnetic nanoparticles and their application as catalyst supports in organic transformations. He completed a postdoctoral fellowship under the supervision of Professor Ali Morsali in 2024, including the design and synthesis of the Chiral Metal–Organic Frameworks (MOFs). Now, he is working as a postdoctoral researcher at the University of the Zanjan under the supervision of Professors Ali Ramazani and Professors Ali Morsali on the design and synthesis of the Chiral Metal–Organic Frameworks (MOFs.

Shaghayegh Fadaei received her B.Sc. in Applied Chemistry from the University of Zanjan in 2022 and completed her M.Sc. in Organic Chemistry at the same university in 2025 under the supervision of Prof. Ali Ramazani. Her Master's thesis focused on the green synthesis of magnetic nanocatalysts and their application in multicomponent reactions. Her research interests include sustainable synthesis, nanocatalysis, and eco-friendly catalytic systems.

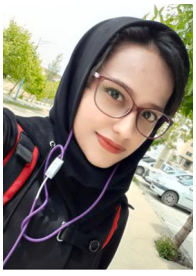

Maryam Manafi Moghadam was born in 1994 in Tehran, Iran. She earned her Bachelor's degree in Applied Chemistry from Damghan University, Damghan, Semnan, Iran, in 2016. She subsequently completed her Master's degree in Organic Chemistry at the same institution in 2018 under the supervision of Dr. Mehdi Zamani. Currently, she is pursuing a Ph.D. in Chemistry at the University of Zanjan, where she works in the research laboratories of Prof. Ali Ramazani and Prof. Ali Morsali. Her research focuses on the design and development of magnetic nanocomposites, specifically their application as catalyst supports in various organic transformations. Her research interests include multi-component reactions (MCRs), the development and application of novel reagents in organic synthesis, the design and characterization of solid acid catalysts, organic reactions, green chemistry, and computational chemistry.

Ali Ramazani completed his PhD under the supervision of Professor Issa Yavari in the Department of Chemistry at the Tarbiat Modares University (TMU) in Tehran-Iran. He currently works as a full professor of chemistry at the University of Zanjan in Zanjan, Iran. His studies are focused on organic synthesis, medicinal chemistry, and nanochemistry, and he has published more than 600 papers and patents. He is an Editorial Board Member of the International Journal of Nanochemistry Research. He has received several national and international awards, including the 2013 Khwarizmi International Award, the national Best Researcher award, the national Distinguished Professor Award, several top-cited author awards, and best-paper awards from leading ISI Journals, Best Researcher Awards, and the Best Lecturer Awards at the University of Zanjan. Google Scholar: https://scholar.google.co.in/citations? user=XDWRu9gAAAAJ&hl=en, https://www.znu.ac.ir/members/ramazani-ali/en.

Yavar Ahmadi was born in 1983 in Marand, Iran. He received his Bachelor's degree in Chemistry and Master's degree in Organic Chemistry in 2006 and 2008, respectively. He received his Ph.D. degree in 2012 from the University of the Zanjan under the supervision of Professor Ali Ramazani. His Ph.D. studies include Multi-component reactions of (N-isocyanimino) triphenylphosphorane in the presence of ketones. He currently works as a Assistant professor of chemistry at the University of Frahangian in Tehran, Iran. His studies are focused on organic synthesis, medicinal chemistry, and nanochemistry, and he has published more than 60 papers. He has received several national awards, including Distinguished Ph.D. Student in Iran, 2012, Awarded by His Excellency the President of Islamic Republic of Iran and the Best Lecturer Awards at the farhangian University. Google Scholar: https://scholar.google.com/citations?user=5RElS30AAAAJ&hl=en, https://orcid.org/0000-0002-4644-7794.

Guoying Zhang earned his PhD in Physical Chemistry from the State Key Laboratory of Oxo Synthesis and Selective Oxidation at the Lanzhou Institute of Chemical Physics, Chinese Academy of Sciences (CAS), under the esteemed mentorship of Professor Hanmin Huang. He further advanced his academic pursuits by completing postdoctoral research in Inorganic Chemistry at the Universität Bayreuth in Germany, where he was guided by the eminent Professor Rhett Kepme. He currently holds the distinguished position of Full Professor in Chemistry and Materials at the State Key Laboratory of Coal Conversion, Institute of Coal Chemistry CAS. His research interests are centered on the efficient low-carbon conversion and utilization of coal-based resources, as well as the green energy conversion and storage technologies. To date, he has contributed to over 80 scholarly papers and patents. He has been the proud recipient of a distinguished array of national and international accolades, including the National Scholarship, the Outstanding Graduate from the CAS, thePresident's Outstanding Prize of CAS, the Humboldt Fellowship, and the 2021 Hundred Talents Program of CAS.